



Molecular Gas in the Outflow of the Small Magellanic Cloud

Enrico M. Di Teodoro¹, N. M. McClure-Griffiths¹, C. De Breuck², L. Armillotta¹, N. M. Pingel¹, K. E. Jameson¹,
John M. Dickey³, M. Rubio⁴, S. Stanimirović⁵, and L. Staveley-Smith^{6,7}

¹ Research School of Astronomy and Astrophysics, The Australian National University, Canberra, ACT 2611, Australia; enrico.diteodoro@anu.edu.au

² European Southern Observatory, Karl-Schwarzschild-Str. 2, D-85748 Garching bei München, Germany

³ School of Natural Sciences, University of Tasmania, Hobart TAS, Australia

⁴ Departamento de Astronomía, Universidad de Chile, Casilla 36, Santiago de Chile, Chile

⁵ Department of Astronomy, University of Wisconsin, Madison, WI 53706, USA

⁶ International Centre for Radio Astronomy Research (ICRAR), University of Western Australia, Crawley, WA 6009, Australia

⁷ ARC Centre of Excellence for All Sky Astrophysics in 3 Dimensions (ASTRO 3D), Australia

Received 2019 August 20; revised 2019 October 18; accepted 2019 October 21; published 2019 November 6

Abstract

We report the first evidence of molecular gas in two atomic hydrogen (HI) clouds associated with gas outflowing from the Small Magellanic Cloud (SMC). We used the Atacama Pathfinder Experiment to detect and spatially resolve individual clumps of $^{12}\text{CO}(2 \rightarrow 1)$ emission in both clouds. CO clumps are compact (~ 10 pc) and dynamically cold (line widths $\lesssim 1$ km s $^{-1}$). Most CO emission appears to be offset from the peaks of the HI emission, some molecular gas lies in regions without a clear HI counterpart. We estimate a total molecular gas mass of $M_{\text{mol}} \simeq 10^3\text{--}10^4 M_{\odot}$ in each cloud and molecular gas fractions up to 30% of the total cold gas mass (molecular + neutral). Under the assumption that this gas is escaping the galaxy, we calculated a cold gas outflow rate of $\dot{M}_{\text{gas}} \simeq 0.3\text{--}1.8 M_{\odot} \text{ yr}^{-1}$ and mass loading factors of $\beta \simeq 3\text{--}12$ at a distance larger than 1 kpc. These results show that relatively weak starburst-driven winds in dwarf galaxies like the SMC are able to accelerate significant amounts of cold and dense matter and inject it into the surrounding environment.

Unified Astronomy Thesaurus concepts: [Small Magellanic Cloud \(1468\)](#); [Magellanic Clouds \(990\)](#); [Interstellar medium \(847\)](#); [Interstellar phases \(850\)](#); [Molecular gas \(1073\)](#); [CO line emission \(262\)](#); [Stellar feedback \(1602\)](#); [Galaxy winds \(626\)](#)

1. Introduction

Galactic outflows powered by either active galactic nuclei (AGN) or star formation feedback have been observed in many galaxies (e.g., Veilleux et al. 2005). Winds have a primary impact in many aspects of galaxy evolution, for example, in regulating the efficiency of star formation and in enriching the circumgalactic medium with metals (Zhang 2018 for a review). The multiphase nature of gas in outflows, from the hot highly ionized phase (10^{6-7} K) down to the cold molecular phase (< 100 K), has been confirmed both by observations (e.g., Arribas et al. 2014; Leroy et al. 2015; Martín-Fernández et al. 2016) and by numerical simulations (e.g., Tanner et al. 2016; Kim & Ostriker 2018; Armillotta et al. 2019).

Because of their shallow gravitational potential, dwarf galaxies are particularly sensitive to supernovae (SNe) explosions and stellar winds and can easily generate galactic winds. Simulations of galaxy evolution with stellar feedback predict that dwarf galaxies can expel large amounts of gas on kiloparsec scales and that cool gas ($T < 10^4$ K) contains most to half of the mass of the outflow (e.g., Hopkins et al. 2012; Muratov et al. 2015). Tidal interactions and mergers can cause bursts of star formation that furthermore power the outflow (Hopkins et al. 2013). Being the closest pair of interacting dwarf galaxies, the Magellanic Clouds constitute unique laboratories to study on parsec scales stellar feedback in action in non-isolated gas-rich dwarf galaxies.

Recently, McClure-Griffiths et al. (2018, hereafter MCG18) demonstrated for the first time that a significant amount of neutral gas is outflowing from the main body of the Small Magellanic Cloud (SMC). Using high-resolution atomic hydrogen (HI) emission-line data with the Australian Square

Kilometre Array Pathfinder (ASKAP), they detected a population of clouds and filaments consistent with being gas driven out by the intense star formation regions in the SMC. They estimated an HI mass in the outflow of $\sim 10^7 M_{\odot}$, about 3% of the total atomic gas mass of the galaxy, with an HI outflow rate of $0.2\text{--}1 M_{\odot} \text{ yr}^{-1}$, i.e., 2–10 times larger than the galaxy star formation rate (SFR). However, the amount of molecular gas entrained in the outflow, which is expected to be significant, is still unconstrained.

In this work, we quantify the contribution of molecular gas to the mass-loss budget in the SMC outflow. We use the Atacama Pathfinder Experiment (APEX; Güsten et al. 2006) telescope to detect and study $^{12}\text{CO}(2 \rightarrow 1)$ emission in two outflowing HI clouds. In the remainder of this Letter, we introduce our new APEX observations in Section 2, we describe our main findings in Section 3 and discuss them in Section 4, summarizing in Section 5. Throughout this Letter, we assume a distance for the SMC of $D = 63 \pm 3$ kpc, for which $10''$ correspond to about 3 pc.

2. Observations

We targeted two HI clouds (SMC-C1 and SMC-C2 hereafter) identified by MCG18 and believed to be material expelled because of star formation feedback. These clouds are among the most prominent and highest-density features with anomalous kinematics in the SMC and they show some intriguing velocity gradients across their structures, suggestive of acceleration. Figure 1 displays a large-scale H α map of the SMC (red color scale) from the Magellanic Cloud Emission-line Survey (MCELS; Winkler et al. 2015), showing several regions of intense star formation. HI column-density maps of

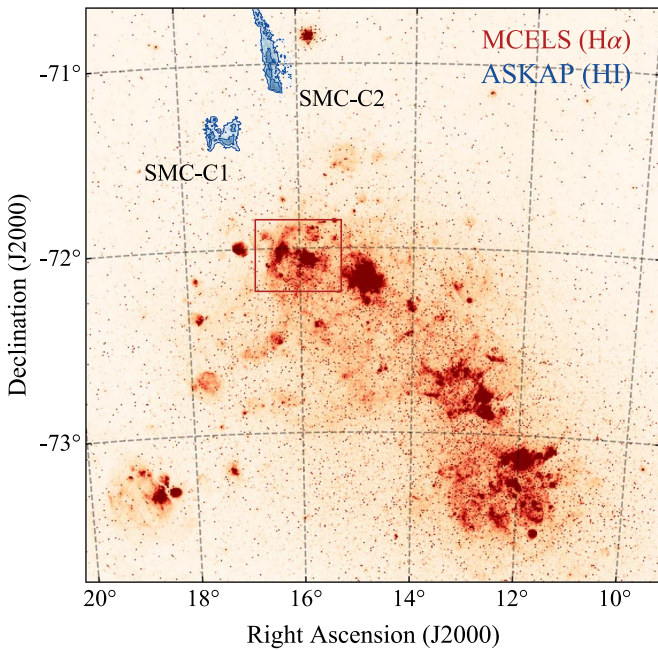


Figure 1. Small Magellanic Cloud (SMC) in $H\alpha$ emission (MCELS survey; Winkler et al. 2015) in red color scale. The two clouds (SMC-C1 and SMC-C2) detected in H I emission (ASKAP; McClure-Griffiths et al. 2018) and targeted in this work are shown in blue color scale. HI contours (blue) are at $(1.0, 2.0) \times 10^{19} \text{ cm}^{-2}$ (SMC-C1) and $(1.5, 2.5) \times 10^{19} \text{ cm}^{-2}$ (SMC-C2). The red box denotes the star formation regions (NGC 371/395) from where the clouds could have been launched.

our targets are overplotted in Figure 1 and shown in detail in Figure 2 (blue color scale). For this work, we mapped the $^{12}\text{CO}(2 \rightarrow 1)$ line with APEX in the regions outlined by the red boxes in Figure 2. Details on the observations and data reduction are given in the Appendix.

3. Results

3.1. Morphokinematics of the CO Emission

Our APEX data show some weak but unequivocal $^{12}\text{CO}(2 \rightarrow 1)$ emission throughout the two fields corresponding to the velocity range of the HI emission, i.e., local standard of rest (LSR) velocity $V_{\text{LSR}} = 90\text{--}115 \text{ km s}^{-1}$ for SMC-C1 and $V_{\text{LSR}} = 120\text{--}140 \text{ km s}^{-1}$ for SMC-C2. To identify regions of genuine emission, we used the 3D source finder implemented in the ^3D BAROLO code (Di Teodoro & Fraternali 2015). In short, the source finder smooths the data to a lower spatial resolution ($50''$ in our case) to improve the signal-to-noise ratio, and reconstructs the sources by merging regions with flux higher than a given threshold ($3 \times \text{rms}$) that are close in both the spatial and the spectral domains. We detected eight main knots or clumps of CO emission in the SMC-C1 field and nine main knots in the SMC-C2 field. A few other regions of low-significance emission were not included in our further analysis.

Figure 2 shows $^{12}\text{CO}(2 \rightarrow 1)$ maps (gray color scale) integrated over the velocity channels showing emission. The detected CO clumps are labeled in red. We overlay the contours of the CO emission on the HI map of Figure 2. In general, in both fields, the peaks of the CO emission are offset from the regions with the highest HI column densities. In SMC-C2, most of the molecular gas is well aligned and shares the kinematics with the neutral gas filament visible in HI. The CO

emission in SMC-C1 has lower signal to noise and the association with the HI emission is not as striking as in SMC-C2: for example, clumps 1, 2, and 7 are located in regions with no or very low column-density neutral gas; clump 4 does not match the kinematics of the adjacent HI gas and has a velocity about 10 km s^{-1} lower than the HI emission. Typical sizes of the CO clumps are of the order of 10 pc.

In Figure 3, we plot spectra for some representative CO knots in SMC-C1 (left panels, clumps 3, 5, 7, and 8) and in SMC-C2 (right panels, clumps 2, 3, 6, and 9). Spectra are integrated over circular regions with a radius of 0.7 centered on the emission peak. CO emission lines are clearly detected. The spectral range corresponding to each detection reconstructed by the source finder is highlighted in gray. We also plot HI spectra (blue histograms) in the same regions extracted from new, high spectral resolution (0.5 km s^{-1}), ASKAP HI data (N. M. Pingel et al. 2019, in preparation). Some of the stronger and more extended knots, like clump 5 in SMC-C1 and clump 2 in SMC-C2, show some velocity gradients across their structure, which results in a relatively broad emission over $1\text{--}2 \text{ km s}^{-1}$ having multiple kinematical components. These knots have velocities in agreement with the broader HI emission. Fainter knots (e.g., clump 8 in SMC-C1 or 9 in SMC-C2) have very narrow, single-component emission, with FWHM line-broadening lower than 0.5 km s^{-1} and can be offset in velocity from the HI emission. In general, all CO clumps have modest line widths, suggesting that turbulence does not play an important role in shaping the molecular gas in the wind.

The main properties of the CO knots are listed in Table 1. Central velocities (column 2), line widths (column 3), and integrated flux densities (column 4) are measured through a Gaussian fit of the spectrum integrated over the entire 3D detection. The radius (column 6) of a clump is calculated as $R_c = D \tan(\sqrt{\Omega_s}/\pi)$, where Ω_s is the area covered by all detected pixels in the integrated intensity map.

3.2. Molecular Gas Mass

We used CO line luminosities and a CO-to- H_2 conversion factor α_{CO} to calculate the molecular gas mass M_{mol} of detected clumps, i.e., $M_{\text{mol}} = \alpha_{\text{CO}} L_{\text{CO}}$ (see Bolatto et al. 2013b for a comprehensive review). We converted from the integrated intensity F_{CO} to CO luminosity L_{CO} as (e.g., Solomon et al. 1997)

$$\frac{L_{\text{CO}}}{(\text{K km s}^{-1} \text{ pc}^2)} = 23.5 \frac{F_{\text{CO}}}{(\text{K km s}^{-1})} \frac{\Omega_s}{(\text{arcs})^2} \left(\frac{D}{\text{Mpc}} \right)^2, \quad (1)$$

where Ω_s is the area covered by a clump on the sky and we use a distance $D = 0.063 \text{ Mpc}$. CO luminosities are listed in column 5 of Table 1. The values of the CO-to- H_2 conversion factors have been extensively studied in self-gravitating molecular clouds in the Milky Way ($\alpha_{\text{CO}} \simeq 4\text{--}5 M_{\odot} (\text{K km s}^{-1} \text{ pc}^2)^{-1}$; e.g., Heyer et al. 2009) and in low-metallicity environments like the SMC ($\alpha_{\text{CO}} \simeq 15\text{--}17 M_{\odot} (\text{K km s}^{-1} \text{ pc}^2)^{-1}$; e.g., Jameson et al. 2018). However, molecular gas in outflows is expected to have very different physical conditions, in terms of density, temperature, and pressure, and robust conversion factors have not been established yet. Some clues that molecular gas in starburst-driven outflows may be in a lower-density and optical-depth state than regular molecular clouds come from CO observations of nearby galaxies M82 (e.g., Weiß et al. 2005) and

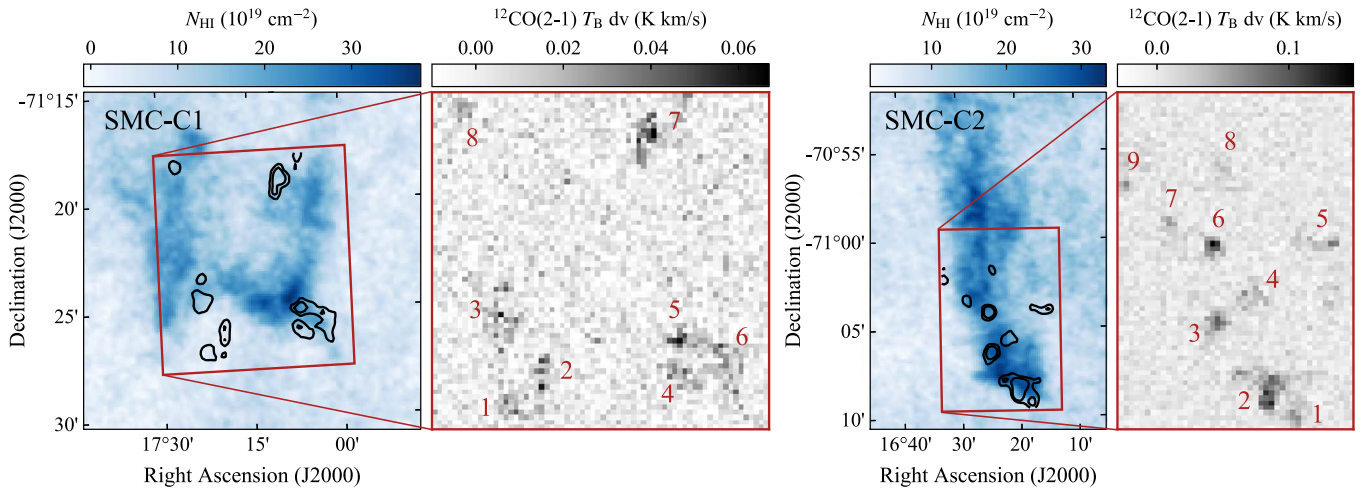


Figure 2. H I and CO maps of SMC-C1 (left panels) and SMC-C2 (right panels). Column-density maps of the H I emission from ASKAP observations (McClure-Griffiths et al. 2018), integrated over the velocity range 90–115 km s⁻¹ (SMC-C1) and 120–140 km s⁻¹ (SMC-C2), are shown in blue color scale. The fields mapped in the ¹²CO(2 → 1) emission line with APEX are delimited with red boxes. Gray scale maps represent the integrated intensity of the ¹²CO(2 → 1) emission line. We identify eight clumps of molecular gas in the SMC-C1 field and nine in SMC-C2, labeled in red in the CO maps. On the H I maps, we overlay the CO contours at levels of [0.02, 0.04] K km s⁻¹.

NGC 253 (e.g., Walter et al. 2017). A few studies on starburst-driven (e.g., Leroy et al. 2015) and AGN-driven outflows (e.g., Cicone et al. 2018) suggest $\alpha_{\text{CO}} \sim 1\text{--}2 M_{\odot} (\text{K km s}^{-1} \text{pc}^2)^{-1}$, lower than the typical values in the Milky Way.

To partially overcome the uncertainties on the CO-to-H₂ conversion, we adopt two representative conversion factors. First, we calculate lower limits to the molecular gas mass assuming that CO gas is optically thin (see, e.g., Bolatto et al. 2013a). In this case, we calculated conversion factors for the CO $J = 2 \rightarrow 1$ transition through Equation (18) from Bolatto et al. (2013b), setting an energy of the $J = 2$ level of $E_2/k = 16.6$ K and assuming an excitation temperature of $T_{\text{ex}} = 30$ K (e.g., Goldsmith 2013). We obtained an $\alpha_{\text{thin}} \simeq 0.12 M_{\odot} (\text{K km s}^{-1} \text{pc}^2)^{-1}$, about two orders of magnitude lower than typical conversion factors in the SMC. Second, we applied the conversion factor $\alpha_{\text{thick}} \simeq 2 M_{\odot} (\text{K km s}^{-1} \text{pc}^2)^{-1}$ estimated in local outflows (e.g., Leroy et al. 2015; Cicone et al. 2018), under the assumption that ¹²CO(2 → 1) is optically thick and thermalized with ¹²CO(1 → 0) (e.g., Rubio et al. 1993). These two conversion factors should give us a plausible range of mass for the molecular gas entrained in the SMC outflow.

The last two columns of Table 1 list the molecular gas masses calculated through α_{thin} and α_{thick} . Typical masses in the optically thin case are of some tens of M_{\odot} , while they span between hundreds and a few thousands of M_{\odot} in the optically thick regime. The total molecular gas mass in the SMC-C1 field is $\sim 500 M_{\odot}$ and $\sim 8 \times 10^3 M_{\odot}$ in the optically thin and thick cases, and $\sim 420 M_{\odot}$ and $\sim 7 \times 10^3 M_{\odot}$ for the SMC-C2 field. We stress again that masses calculated through α_{thin} represent lower limits. Considering that it is unlikely that the CO line is completely optically thin, we can conclude that the mass of molecular gas in both fields is sensibly in the range $10^3\text{--}10^4 M_{\odot}$.

The low metallicity of the SMC could imply larger α_{CO} (thus larger molecular gas masses) than the α_{thick} estimated in local outflows and assumed so far. As a sanity check, we calculated the masses that our CO clouds would have in case of virial equilibrium (see Bolatto et al. 2013b), which therefore may represent upper limits to the molecular gas mass for non-self-gravitating clouds entrained in an outflow. The optically thick

masses calculated with α_{thick} are consistent with the virial masses for spherical clouds with density $\rho(r) \propto r^{-2}$ and about $\sim 30\%$ lower than virial masses for clouds with $\rho(r) \propto r^{-1}$. This suggests that our molecular masses are not significantly underestimated and that the α_{CO} for these CO clumps is likely closer to the $2 M_{\odot} (\text{K km s}^{-1} \text{pc}^2)^{-1}$ estimated in local outflows rather than to the $\sim 16 M_{\odot} (\text{K km s}^{-1} \text{pc}^2)^{-1}$ found in the main body of the SMC.

4. Discussion

MCG18 discusses that the most likely interpretation for these H I clouds is a star formation-driven outflow. The anomalous kinematics alone would not provide a conclusive argument on the origin of this gas. For example, gas accreting onto the galaxy from the surrounding environment (Sancisi et al. 2008) and gas stripped because of tidal interactions or because of ram pressure due to the motion of the SMC through the Milky Way halo (Gunn et al. 1972) could easily present peculiar kinematics. However, quite compelling evidence in support of the outflow interpretation is the association of these H I features with H α shells arising from the star-forming regions in the SMC (see MCG18 for details). The detection of CO in both fields studied in this work provides further support to the outflow scenario: molecular gas is not observed in H I clouds associated with extragalactic accreting gas (like high-velocity clouds; e.g., Dessauges-Zavadsky et al. 2007) and the thermal pressure in a Milky Way-like halo does not seem high enough to confine stripped gas to the high densities typical of molecular material (e.g., see discussion in Tonnesen & Bryan 2012). However, because we cannot constrain the real geometry of the system, we do not know whether the gas is escaping the galaxy or if it is falling back through a galactic fountain mechanism (Fraternali 2017). MCG18 pointed out that the observed velocity in these clouds is likely large enough to escape the shallow gravitational potential of the SMC.

How hot winds can accelerate cold gas to the observed velocities is still a debated question. Several recent simulations of individual cold clouds entrained in a hot, supersonic flow showed that a cloud is easily shredded during the acceleration

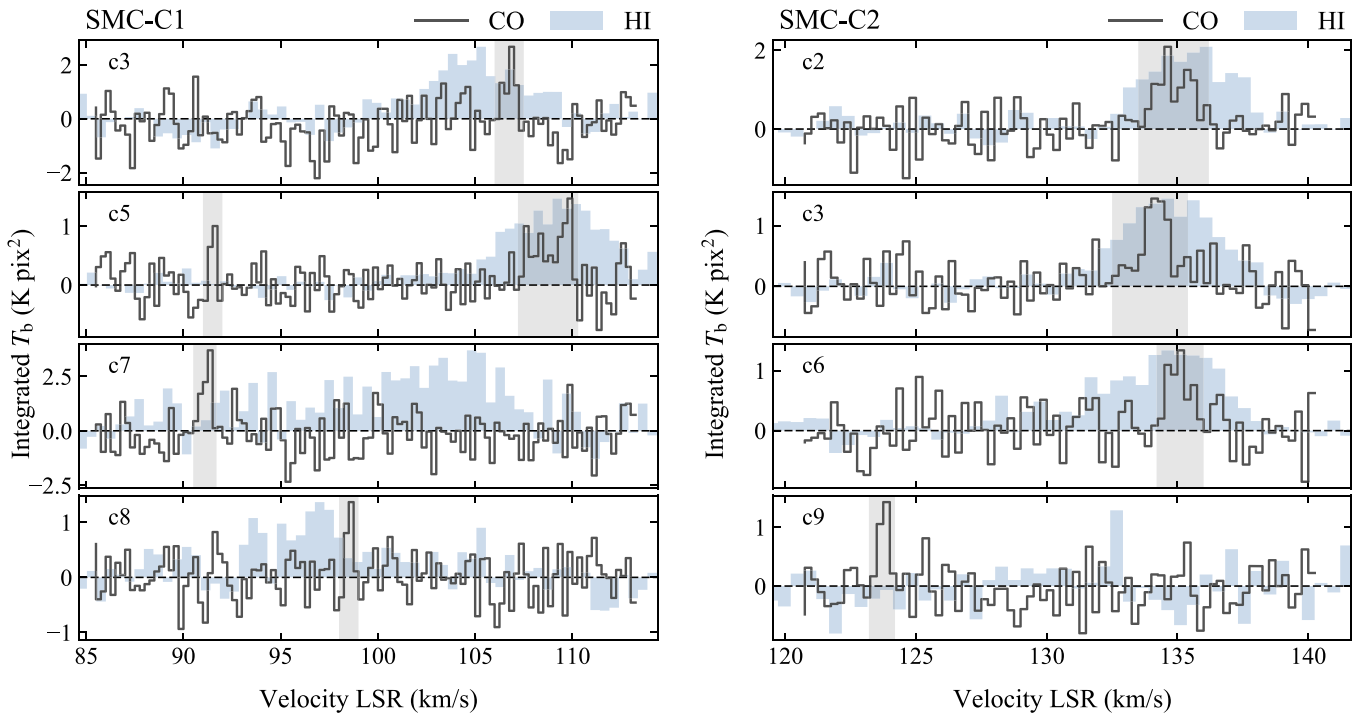


Figure 3. Spectra of the main clumps of $^{12}\text{CO}(2 \rightarrow 1)$ emission (black line) detected with APEX for SMC-C1 (left panels) and SMC-C2 (right panels). Spectra are integrated over a 0.7 circular aperture. The velocity range of each detection is highlighted in gray. The narrow emission line at $V_{\text{LSR}} \simeq 91 \text{ km s}^{-1}$ visible in the SMC-C1’s clump 5 spectrum is contaminated from the nearby, spectrally decoupled, clump 4. Light blue histograms denote H I spectra integrated on the same aperture and normalized to the CO peak for a easier visualization.

process on short timescales (e.g., Scannapieco & Brüggén 2015; Gronke & Oh 2018; Sparre et al. 2019). Although these simulations do not trace the cold molecular phase, the general expectation is of a head–tail cloud morphology, with the densest and coldest core in the trailing head of the cloud and the shredded warmer envelope in the leading tail. Our CO and H I observations are qualitatively in agreement with this scenario: if our clouds were launched from the closest prominent star formation region in the SMC, i.e., NGC 371/395, located southwest of SMC-C1 and south–southwest of SMC-C2 (see the red box in Figure 1), the densest CO clumps in our data (4, 5, and 6 in SMC-C1, 1 and 2 in SMC-C2) would represent the compact core of the initial cloud following the fragmented mixture of molecular and neutral gas. In this scenario, the spatial distributions of neutral and molecular gas and the observed offsets are signatures of the cloud disruption and of the interaction between cold gas and the hot flow. A puzzling aspect that emerges from our observations and seems to hinder the entrainment interpretation is the very narrow line widths observed in the molecular gas ($\sim 1 \text{ km s}^{-1}$): velocity dispersions are expected to increase while cold gas is shocked and shredded by the hot flow (Banda-Barragán et al. 2019). New simulations aimed to trace properly the molecular phase of the outflow are needed to address this observational evidence. The small line widths may imply that we are only observing the innermost region of a molecular cloud that is not (yet) directly interacting with the wind.

The total mass of molecular gas in both our targets is 10^3 – $10^4 M_{\odot}$. The amount of neutral gas (H+He) estimated from the H I ASKAP observations in the same regions of our APEX fields is $4.0 \times 10^4 M_{\odot}$ for SMC-C1 and $3.3 \times 10^4 M_{\odot}$ for SMC-C2. This leads to molecular gas fractions $f_{\text{mol}} = M_{\text{mol}}/(M_{\text{HI}} + M_{\text{mol}}) \simeq 0.03$ – 0.30 , i.e., the contribution in

mass of molecular gas to the total outflowing material ranges from a few percent up to $\sim 30\%$. MCG18 estimated an outflow rate in H I of $\dot{M}_{\text{HI}} \simeq 0.2$ – $1 M_{\odot} \text{ yr}^{-1}$ (~ 0.3 – $1.4 M_{\odot} \text{ yr}^{-1}$ including helium), assuming that the outflowing gas originated from the most recent burst of star formation in the SMC, between 25 and 60 Myr ago (e.g., Rubele et al. 2015). If the molecular gas fractions derived in this work hold for all the anomalous H I features found by MCG18, the cold gas (neutral + molecular) outflow rate adds up to a value $\dot{M}_{\text{gas}} \sim 0.3$ – $1.8 M_{\odot} \text{ yr}^{-1}$. If only 40% of the ejecta have velocities exceeding the escape velocity from the galaxy (see MCG18), the SMC may lose its entire cold gas reservoir, i.e., $\sim 6 \times 10^8 M_{\odot}$ of neutral gas (e.g., Stanimirovic et al. 1999) and $\sim 3 \times 10^7 M_{\odot}$ of molecular gas (e.g., Rubio et al. 1993), on timescales of $t_{\text{dep}} = 0.9$ – 3 Gyr . We speculate that this large amount of cold gas expelled from the SMC may feed and enrich the Magellanic Stream and the circumgalactic medium of the Milky Way.

Finally, we can estimate a cold mass loading factor of $\beta \equiv \dot{M}_{\text{gas}}/\text{SFR} \simeq 3$ – 12 , where $\text{SFR} \simeq 0.15 M_{\odot} \text{ yr}^{-1}$ is the average star formation rate during the period 25–60 Myr ago (e.g., Rubele et al. 2015). Comparing these numbers to simulations of SN-driven winds in dwarf galaxies is not straightforward because mass loading factors are a function of the distance from the wind launching region. In addition, most simulations do not appropriately trace neutral and molecular gas phases and quoted loading factors often include the hot ionized phase. If we assume that our clouds started their journey from the NGC 371 region, we have angular separations of $\sim 0.8^{\circ}$ and $\sim 1^{\circ}$ for SMC-C1 and SMC-C2, respectively, corresponding to projected distances of $\sim 0.9 \text{ kpc}$ and $\sim 1.1 \text{ kpc}$. These are lower limits to the actual distances, which are unconstrainable due to the unknown geometry of the

Table 1
Properties of the CO Clumps in SMC-C1 (a) and SMC-C2 (b)

| (a) SMC-C1 | | | | | | | |
|------------|--|--------------------------------|---|---|---------------|------------------------------|-------------------------|
| # | V_{LSR} (km s^{-1}) | FWHM (km s^{-1}) | F_{CO} (K km s^{-1}) | L_{CO} ($\text{K km s}^{-1} \text{pc}^2$) | R_c (pc) | $M_{\text{mol}} (M_{\odot})$ | |
| | | | | | | α_{thin} | α_{thick} |
| 1 | 91.89 ± 0.12 | 1.11 ± 0.18 | 1.12 ± 0.36 | 326.4 ± 124.2 | 10 ± 2 | 39 ± 14 | 652 ± 248 |
| 2 | 93.12 ± 0.14 | 0.28 ± 0.19 | 0.46 ± 0.32 | 150.1 ± 111.9 | 11 ± 2 | 18 ± 13 | 300 ± 223 |
| 3 | 106.98 ± 0.18 | 0.48 ± 0.18 | 1.34 ± 0.52 | 645.9 ± 299.3 | 13 ± 2 | 77 ± 35 | 1291 ± 598 |
| 4 | 91.56 ± 0.11 | 0.40 ± 0.15 | 1.09 ± 0.42 | 373.6 ± 170.3 | 11 ± 2 | 44 ± 20 | 747 ± 340 |
| 5 | 108.75 ± 0.15 | 1.52 ± 0.16 | 2.36 ± 0.43 | 1186.4 ± 294.5 | 13 ± 2 | 142 ± 35 | 2372 ± 588 |
| 6 | 110.26 ± 0.12 | 0.31 ± 0.16 | 0.57 ± 0.32 | 114.0 ± 77.3 | 8 ± 2 | 13 ± 9 | 227 ± 154 |
| 7 | 91.28 ± 0.15 | 0.88 ± 0.18 | 1.85 ± 0.53 | 1184.3 ± 418.4 | 15 ± 2 | 142 ± 50 | 2368 ± 836 |
| 8 | 98.67 ± 0.12 | 0.34 ± 0.14 | 0.67 ± 0.31 | 184.7 ± 92.8 | 10 ± 1 | 22 ± 11 | 369 ± 185 |
| (b) SMC-C2 | | | | | | | |
| # | V_{LSR} (km s^{-1}) | FWHM (km s^{-1}) | F_{CO} (K km s^{-1}) | L_{CO} ($\text{K km s}^{-1} \text{pc}^2$) | R_c (pc) | $M_{\text{mol}} (M_{\odot})$ | |
| | | | | | | α_{thin} | α_{thick} |
| 1 | 135.34 ± 0.14 | 0.66 ± 0.18 | 1.15 ± 0.35 | 372.1 ± 141.7 | 11 ± 2 | 44 ± 17 | 744 ± 283 |
| 2 | 135.08 ± 0.18 | 1.56 ± 0.19 | 2.56 ± 0.52 | 1175.1 ± 296.6 | 13 ± 1 | 141 ± 35 | 2350 ± 593 |
| 3 | 134.41 ± 0.16 | 0.99 ± 0.18 | 1.71 ± 0.44 | 585.1 ± 189.8 | 11 ± 2 | 70 ± 22 | 1170 ± 379 |
| 4 | 130.96 ± 0.13 | 0.63 ± 0.15 | 0.97 ± 0.28 | 404.3 ± 135.6 | 12 ± 1 | 48 ± 16 | 808 ± 271 |
| 5 | 131.50 ± 0.14 | 0.56 ± 0.16 | 0.91 ± 0.34 | 294.4 ± 121.9 | 11 ± 1 | 35 ± 14 | 588 ± 243 |
| 6 | 135.13 ± 0.11 | 1.03 ± 0.14 | 1.34 ± 0.34 | 388.9 ± 120.4 | 10 ± 1 | 46 ± 14 | 777 ± 240 |
| 7 | 132.09 ± 0.14 | 0.82 ± 0.13 | 0.63 ± 0.27 | 152.7 ± 72.8 | 9 ± 1 | 18 ± 8 | 305 ± 145 |
| 8 | 123.56 ± 0.18 | 0.25 ± 0.19 | 0.54 ± 0.42 | 194.1 ± 157.0 | 11 ± 2 | 23 ± 18 | 388 ± 313 |
| 9 | 123.92 ± 0.19 | 0.33 ± 0.21 | 0.85 ± 0.55 | 337.8 ± 238.7 | 12 ± 2 | 40 ± 28 | 675 ± 477 |

Note. Columns: (1) clump number; (2)–(3) central velocity (LSR) and FWHM line width of the integrated CO line; (4) integrated flux density; (5) CO luminosity; (6) clump size in radius $R_c = D \tan(\sqrt{\Omega_s/\pi})$ (see the text); (7) molecular mass using an $\alpha_{\text{CO}} = 0.12 M_{\odot} (\text{K km s}^{-1} \text{pc}^2)^{-1}$, i.e., optically thin regime for the $^{12}\text{CO}(2 \rightarrow 1)$ transition; (8) molecular mass using an $\alpha_{\text{CO}} = 2 M_{\odot} (\text{K km s}^{-1} \text{pc}^2)^{-1}$. Errors are propagated from the uncertainties of the Gaussian fit to the integrated spectrum of each knot.

ejected gas. Since most of the HI outflowing clouds in MCG18 lie at projected distances $\gtrsim 1$ kpc from the closest star formation regions, our estimated loading factor is measured at $R > 1$ kpc. The general theoretical expectation is that dwarf galaxies drive out gas at a rate much higher than their SFR, i.e., $\beta \gg 1$. For examples, cosmological simulations by Hopkins et al. (2012) and Muratov et al. (2015) returned loading factors (including the hot phase) at $R > 500$ pc of $\beta \sim 8$ –20 for SMC-like dwarf galaxies. Recent high-resolution simulations of SN-driven winds in isolated dwarf galaxies by Hu (2019) found $\beta \sim 1$ –10 for the warm gas component ($T < 3 \times 10^4$ K) at $R > 1$ kpc. Although the exact values of loading factors depend also on the initial conditions for the gas (e.g., density, metallicity, thickness of the disk) and on the prescriptions adopted for star formation and SN feedback, we can conclude that the cold mass loading factor $\beta = 3$ –12 estimated in this work is broadly consistent with those found in simulations.

5. Conclusions

This Letter presented the first study of molecular gas associated with the outflow of the Small Magellanic Cloud through the detection of the $^{12}\text{CO}(2 \rightarrow 1)$ emission line with the APEX telescope. Thanks to the relatively small distance of the SMC, we spatially resolved individual knots of CO emission in two outflowing HI clouds. CO clumps are compact (~ 10 pc), cold, and nonturbulent, with typical integrated line-broadening of less than 1 km s^{-1} . Most CO clumps do not

overlap but they are slightly offset from the densest HI regions, in qualitative agreement with expectations from simulations of cold clouds entrained in a hot wind. We estimated molecular gas masses in optically thin ($\alpha_{\text{CO}} = 0.12 M_{\odot} (\text{K km s}^{-1} \text{pc}^2)^{-1}$) and optically thick outflow ($\alpha_{\text{CO}} = 2 M_{\odot} (\text{K km s}^{-1} \text{pc}^2)^{-1}$) regimes and we ended up with a range of masses $M_{\text{mol}} = 10^3$ – $10^4 M_{\odot}$ for both the observed fields, with molecular to total cold gas fractions between 0.03 and 0.30. Assuming an outflow interpretation, we estimated a total outflow rate of 0.3–1.8 M_{\odot} for the cold gas component, implying that the SMC may expel the majority of its present-day cold gas reservoir in a few Gyr. The estimated cold mass loading factor $\beta \simeq 3$ –12 at $R > 1$ kpc is overall consistent with simulations of SN-driven winds in dwarf galaxies.

E.D.T. thanks Alberto Bolatto for his useful comments and P. F. Winkler for providing MCELS data. E.D.T. and N.M.-G. acknowledge the support of the Australian Research Council through grant DP160100723. M.R. wishes to acknowledge support from CONICYT(CHILE) through FONDECYT grant No1140839 and partial support from CONICYT project Basal AFB-170002. APEX is a collaboration between the Max-Planck-Institut für Radioastronomie, the European Southern Observatory, and the Onsala Space Observatory.

Facilities: APEX(PI230), ASKAP.


Software: CLASS/GILDAS (Gildas Team 2013), ^3D BAROLO (Di Teodoro & Fraternali 2015).

Appendix Observations and Data Reduction

Submillimeter observations were made using the 12 m APEX telescope in 2019 June (ESO project ID 0103.B-0120A; PI: E. M. Di Teodoro). The weather conditions were stable and dry, with a precipitable water vapor $PWV = 0.6\text{--}1.5$ mm. The PI230 heterodyne receiver was tuned to map the $^{12}\text{CO}(2 \rightarrow 1)$ emission line at 230.538 GHz. The fourth-generation fast-Fourier transform spectrometer (dFFTS4G; Klein et al. 2012) backend connected to the receiver provided a bandwidth of 8 GHz with a spectral resolution of 61 kHz, corresponding to a velocity resolution of about 0.08 km s^{-1} at 230 GHz. At this frequency, the beam size is $\theta = 26''/3$ (FWHM), the main-beam efficiency is $\eta_{\text{mb}} \simeq 0.72$, and the Jy K^{-1} conversion factor is 40 ± 3 .⁸ We observed our targets in on-the-fly total-power mode, sampling every $9''$ with an integration time of 1 s. For SMC-C1, we mapped a $10' \times 10'$ region centered at $(\alpha, \delta)_{\text{J2000}} = (01^{\text{h}}08^{\text{m}}58^{\text{s}}.0, -71^{\circ}22'39'')$; for SMC-C2, we mapped a $7' \times 10'$ region centered at $(\alpha, \delta)_{\text{J2000}} = (01^{\text{h}}05^{\text{m}}31^{\text{s}}.0, -71^{\circ}04'26'')$. Observed regions are shown as red boxes in Figure 2. Integration times were 25 hr and 17 hr for SMC-C1 and SMC-C2, respectively, including calibrations and overheads.

Data reduction was performed using the Continuum and Line Analysis Single-dish Software (Gildas Team 2013). A first-order baseline was subtracted from calibrated spectra by interpolating the channels outside the velocity windows where we expected to see the emission based on the HI observations. We resampled the spectra with a 0.25 km s^{-1} channel width and mapped them onto a grid with pixel sizes of $9''$. The rms noise in our final data cubes is 37 mK and 32 mK in a 0.25 km s^{-1} channel for SMC-C1 and SMC-C2, respectively.

ORCID iDs

Enrico M. Di Teodoro  <https://orcid.org/0000-0003-4019-0673>
 N. M. McClure-Griffiths  <https://orcid.org/0000-0003-2730-957X>
 C. De Breuck  <https://orcid.org/0000-0002-6637-3315>
 L. Armillotta  <https://orcid.org/0000-0002-5708-1927>
 K. E. Jameson  <https://orcid.org/0000-0001-7105-0994>
 John M. Dickey  <https://orcid.org/0000-0002-6300-7459>
 L. Staveley-Smith  <https://orcid.org/0000-0002-8057-0294>

References

- Armillotta, L., Krumholz, M. R., Di Teodoro, E. M., & McClure-Griffiths, N. M. 2019, *MNRAS*, in press
- Arribas, S., Colina, L., Bellocchi, E., Maiolino, R., & Villar-Martín, M. 2014, *A&A*, **568**, A14
- Banda-Barragán, W. E., Zertuche, F. J., Federrath, C., et al. 2019, *MNRAS*, **486**, 4526
- Bolatto, A. D., Warren, S. R., Leroy, A. K., et al. 2013a, *Natur*, **499**, 450
- Bolatto, A. D., Wolfire, M., & Leroy, A. K. 2013b, *ARA&A*, **51**, 207
- Cicone, C., Severgnini, P., Papadopoulos, P. P., et al. 2018, *ApJ*, **863**, 143
- Dessauges-Zavadsky, M., Combes, F., & Pflammiger, D. 2007, *A&A*, **473**, 863
- Di Teodoro, E. M., & Fraternali, F. 2015, *MNRAS*, **451**, 3021
- Fraternali, F. 2017, in *Gas Accretion onto Galaxies*, ed. A. Fox & R. Davé (Cham: Springer International), 323
- Gildas Team, 2013, GILDAS: Grenoble Image and Line Data Analysis Software, Astrophysics Source Code Library, ascl:1305.010
- Goldsmith, P. F. 2013, *ApJ*, **774**, 134
- Gronke, M., & Oh, S. P. 2018, *MNRAS*, **480**, L111
- Gunn, J. E., Gott, J., & Richard, I. 1972, *ApJ*, **176**, 1
- Güsten, R., Nyman, L. Á., Schilke, P., et al. 2006, *A&A*, **454**, L13
- Heyer, M., Krawczyk, C., Duval, J., & Jackson, J. M. 2009, *ApJ*, **699**, 1092
- Hopkins, P. F., Kereš, D., Murray, N., et al. 2013, *MNRAS*, **433**, 78
- Hopkins, P. F., Quataert, E., & Murray, N. 2012, *MNRAS*, **421**, 3522
- Hu, C.-Y. 2019, *MNRAS*, **483**, 3363
- Jameson, K. E., Bolatto, A. D., Wolfire, M., et al. 2018, *ApJ*, **853**, 111
- Kim, C.-G., & Ostriker, E. C. 2018, *ApJ*, **853**, 173
- Klein, B., Hochgürtel, S., Krämer, I., et al. 2012, *A&A*, **542**, L3
- Leroy, A. K., Walter, F., Martini, P., et al. 2015, *ApJ*, **814**, 83
- Martín-Fernández, P., Jiménez-Vicente, J., Zurita, A., Mediavilla, E., & Castillo-Morales, Á. 2016, *MNRAS*, **461**, 6
- McClure-Griffiths, N. M., Dénes, H., Dickey, J. M., et al. 2018, *NatAs*, **2**, 901
- Muratov, A. L., Kereš, D., Faucher-Giguère, C.-A., et al. 2015, *MNRAS*, **454**, 2691
- Rubele, S., Girardi, L., Kerber, L., et al. 2015, *MNRAS*, **449**, 639
- Rubio, M., Lequeux, J., & Boulanger, F. 1993, *A&A*, **271**, 9
- Sancisi, R., Fraternali, F., Oosterloo, T., & van der Hulst, T. 2008, *A&ARv*, **15**, 189
- Scannapieco, E., & Brüggem, M. 2015, *ApJ*, **805**, 158
- Solomon, P. M., Downes, D., Radford, S. J. E., & Barrett, J. W. 1997, *ApJ*, **478**, 144
- Sparre, M., Pfrommer, C., & Vogelsberger, M. 2019, *MNRAS*, **482**, 5401
- Stanimirovic, S., Staveley-Smith, L., Dickey, J. M., Sault, R. J., & Snowden, S. L. 1999, *MNRAS*, **302**, 417
- Tanner, R., Cecil, G., & Heitsch, F. 2016, *ApJ*, **821**, 7
- Tonnesen, S., & Bryan, G. L. 2012, *MNRAS*, **422**, 1609
- Veilleux, S., Cecil, G., & Bland-Hawthorn, J. 2005, *ARA&A*, **43**, 769
- Walter, F., Bolatto, A. D., Leroy, A. K., et al. 2017, *ApJ*, **835**, 265
- Weiß, A., Walter, F., & Scoville, N. Z. 2005, *A&A*, **438**, 533
- Winkler, P. F., Smith, R. C., Points, S. D. & MCELS Team 2015, in *ASP Conf. Ser. 491, Fifty Years of Wide Field Studies in the Southern Hemisphere: Resolved Stellar Populations of the Galactic Bulge and Magellanic Clouds*, ed. S. Points & A. Kunder (San Francisco, CA: ASP), 343
- Zhang, D. 2018, *Galax*, **6**, 114

⁸ <http://www.apex-telescope.org/telescope/efficiency>